2009 Fall Technical Meeting
Organized by the Eastern States Section of the Combustion Institute
and Hosted by the University of Maryland, College Park
October 18-21, 2009

Assessment of Syngas Kinetic Models for the Prediction of a Turbulent Nonpremixed Flame

Osama A. Marzouk and E David Huckaby

U.S. DOE, National Energy Technology Laboratory

3610 Collins Ferry Road, P.O. Box 880

Morgantown, WV 26507-0880, USA

We consider eight kinetic models for syngas (CO-H_2) oxidation, which have been proposed or used for different applications, such as laminar counter-flow flames and hypersonic engines. The models range in size from 2 global steps to 38 elementary steps. We assess the models performance in predicting a simple turbulent jet flame (Sandia/ETH-Zurich flame A). The fuel consists of CO, H_2, and N_2 with 40%, 30%, and 30% by volume, respectively. We simulate the turbulent flame using the finite volume method and compare the Favre-averaged profiles of temperature and mass fractions of the stable species with the experimental data. These comparisons characterize the applicability of the kinetic models to turbulent flames. Turbulence is modeled using the k-epsilon model with McGuirk-Rodi modification for round jets. Turbulence-chemistry interaction is modeled using the partially stirred reactor (PaSR) approach. The kinetic models vary largely in their computational cost. Five of the models overpredicted the maximum flame temperature (by 200K-320K). The 2-step (Slavinskaya et al., 2005) and 9-step (Edelman-Fortune, 1969) models underpredicted the maximum temperature by 240K and 580K, respectively. Predictions using the 3-step model of Cuoci et al. (2009), which is based on the Westbrook-Dryer (1981) model for hydrocarbon fuels, gave less than 10K difference. This model also has the lowest computational cost.

1 Introduction

The term 'syngas' refers to a gas mixture composed mainly of CO and H_2. It is generated during steam reforming of natural gas to produce hydrogen and during the gasification of coal. The name is derived from *synthesis gas*, which comes from its use as intermediates in producing synthetic natural gas (SNG) [1], synthetic petroleum oil, ammonia, or methanol.

Syngas can be used as a fuel in a combustion turbine to produce electrical or thermal power. We assess the performance of these kinetic models in reproducing the characteristics of a simple $CO/H_2/N_2$ (40%/30%/30% by volume) turbulent nonpremixed flame, examined experimentally by Sandia National Laboratory (scalar measurements) in California and the Swiss Federal Institute of Technology - ETH (velocity measurements) in Zurich. This flame has the advantage of simple geometry, which magnifies the role of the kinetic model in the predictions, and minimizes other factors in the simulations such as the geometric representation and discretization of the domain.

In addition to the benefit described above, the Favre-averaged data are available for this flame [2, 3, 4]. This characteristic avoids the inconsistency inherited in comparing Favre-averaged predictions with Reynolds-averaged measurements. Whereas the experiments of Panda and Seasholtz [5] suggest that the difference between the two types of averaging (Favre and Reynolds) are small for unheated free jets with Mach numbers from 0.8 to 1.8, reactive flows exhibit large density variations [6], and this difference can be non-negligible. Using inconsistent averaging when comparing numerical predictions with measurements leads to uncertainties in interpreting the results [7, 8].

The flame which is used for this study is known as the 'chnA flame'. The lowercase 'chn' stands for carbon monoxide, hydrogen, and nitrogen. The uppercase 'A' refers to the first of two similar flames studied in the experiment. Both flames have the same jet Reynolds number, but the 'A' flame has a smaller burner tube and is more challenging to simulate due to the higher velocity (the area-averaged exit jet velocity here is 76m/s, compared to 45m/s for flame 'B'). A photograph of the flame is given in Figure 1. The burner tube has an inner diameter of 4.58mm and an outer diameter of 6.34mm. Therefore, the thickness is only 0.88mm. However, it was sufficient to stabilize the flame through a small recirculation zone. The fuel-jet Reynolds number (Re_j) at the exit of the burner tube was approximately 16,700. It is defined as

$$\mathrm{Re}_j = \frac{U_j\, d}{\nu_j} \tag{1}$$

where $U_j = 76\mathrm{m/s}$ is the average (bulk) jet velocity, $d = 0.00458\mathrm{m}$ is the inner diameter, and $\nu_j = 2.083 \times 10^{-5}\mathrm{m}^2/\mathrm{s}$ is the kinematic viscosity. The jet exit temperature was 292 K. The coflow air had a velocity of 0.7m/s, a temperature of 290 K, and 1.2% mole fraction of water vapor ($X_{H2O,\mathrm{coflow}}$). Based on the information provided by Sandia, the elemental mass fractions in the coflow, we calculated the mole fractions of oxygen and nitrogen and found them to be $X_{O2,\mathrm{coflow}}$=20.525% and $X_{N2,\mathrm{coflow}}$ =78.275%. Scalar measurements (temperatures and mass fractions) were conducted at Sandia using a combination of spontaneous Raman scattering and Rayleigh scattering.

2 Formulation

The equations for mass, momentum, energy, and species mass conservation [6, 9] are

$$\frac{\partial\,\bar{\rho}}{\partial\,t} + \nabla\cdot(\bar{\rho}\,\tilde{\vec{U}}) = 0 \tag{2}$$

$$\frac{\partial\left(\bar{\rho}\,\tilde{\vec{U}}\right)}{\partial\, t} + \nabla\cdot\left(\bar{\rho}\,\tilde{\vec{U}}\,\tilde{\vec{U}}\right) = -\nabla\bar{p} + \nabla\cdot\left(\tilde{\tau_{\vec{eff}}}\right) + \bar{\rho}\,\vec{g} \tag{3}$$

$$\frac{\partial\left(\bar{\rho}\,\tilde{h}\right)}{\partial\, t} + \nabla\cdot\left(\bar{\rho}\,\tilde{\vec{U}}\,\tilde{h}\right) = \nabla\cdot\left(\alpha_{eff}\,\nabla\tilde{h}\right) + \nabla\cdot\sum_{i=1}^{N_s}\left(\tilde{h}_i\,\nabla\tilde{Y}_i\left[\mu_{eff} - \alpha_{eff}\right]\right) + \frac{\partial\,\bar{p}}{\partial\, t} \tag{4}$$

$$\frac{\partial\left(\bar{\rho}\,\tilde{Y}_i\right)}{\partial\, t} + \nabla\cdot\left(\bar{\rho}\,\tilde{\vec{U}}\,\tilde{Y}_i\right) = \nabla\cdot\left(\mu_{eff}\,\nabla\tilde{Y}_i\right) + \kappa\,\overline{RR}_i \tag{5}$$

The bar denotes a time-averaged value and the tilde denotes a Favre-averaged value, such as

$$\tilde{\phi} \equiv \frac{\overline{\rho\,\phi}}{\bar{\rho}}$$

The Reynolds Stress, τ_{eff} is the sum of the laminar and turbulent stress. Similarly the effective thermal and species flux has been calculated as the sum of the laminar and turbulent fluxes in Equations 4 and 5. The turbulent fluxes have been calculated using the gradient diffusion hypothesis and introduction of a turbulent viscosity and turbulent thermal diffusivity. This particular model assumes that laminar and turbulent Schmidt numbers for all species is unity. The chemical source ($\overline{RR}_i$) of the i^{th} species in Equation (5) is scaled by the reactive volume fraction (κ), which takes a value from 0 to 1. The turbulence-chemistry interaction is modeled based on the partially stirred reactor (PaSR) approach [10, 11], where the computational cell is divided into two zones: a reacting zone which is modeled as a perfectly stirred reactor (PSR) and non-reacting zone. This model is related to the eddy dissipation concept (EDC) model [12, 13]. The reactive volume fraction (κ) is calculated as

$$\kappa = \frac{\tau_{res} + \tau_c}{\tau_{res} + \tau_c + \tau_{mix}} \tag{6}$$

where the residence time (τ_{res}) is equal to the time step (Δt), τ_c is the chemical reaction time, and τ_{mix} is the mixing time

$$\tau_{mix} = C_{mix}\,\sqrt{\frac{\mu_{eff}}{\bar{\rho}\,\tilde{\epsilon}}} \tag{7}$$

For the calculation performed in this paper, the mixing-rate constant (C_{mix}) is unity. The chemical reaction time (τ_c) is calculated from the total molar concentration in the cell and the average (over all reactions) concentration rate of the product species. The specific enthalpy of the i^{th} species is

$$h_i = h_i^o + \int_{T_o}^{T}\left(C_{p,i}\,dT\right) \tag{8}$$

where h_i^o is the heat of formation of the i^{th} species at a reference temperature (T_o), and $C_{p,i}$ is the specific heat at constant pressure for the i^{th} species. Here, T_o=298.15 K. The specific enthalpy of the mixture (h) is the sum of the specific enthalpies of its species (h_i), thus

$$h = \sum_{i=1}^{N_s} h_i Y_i \tag{9}$$

where Y_i is the mass fraction of the i^{th} species and N_s is the number of species. The dynamic thermal diffusivity (α) is defined as

$$\alpha \equiv \lambda/C_p = \frac{\mu}{\mathrm{Pr}} \tag{10}$$

where λ is the thermal conductivity of the mixture, C_p is its specific heat at constant pressure, and Pr is the Prandtl number. Due to the turbulence closure, α is replaced by α_{eff}, where

$$\alpha_{eff} = \alpha + \frac{\mu_t}{\mathrm{Pr}_t} \tag{11}$$

and Pr_t is the turbulent Prandtl number (here $\mathrm{Pr}_t = 1$), and the effective dynamic viscosity (μ_{eff}) is introduced as

$$\mu_{eff} = \mu + \mu_t \tag{12}$$

where the turbulent viscosity (μ_t) is calculated as

$$\mu_t = C_\mu \, \bar{\rho} \, \frac{\tilde{k}^2}{\tilde{\epsilon}} \tag{13}$$

where $\tilde{k}$ and $\tilde{\epsilon}$ are the Favre-averaged turbulent kinetic energy per unit mass and its dissipation rate, respectively. Their transport equations are

$$\frac{\partial \left(\bar{\rho}\,\tilde{k}\right)}{\partial t} + \nabla \cdot \left(\bar{\rho}\,\tilde{\vec{U}}\,\tilde{k}\right) = \nabla \cdot \left(\left[\mu + \frac{\mu_t}{\sigma_k}\right] \nabla \tilde{k}\right) + P - \bar{\rho}\,\tilde{\epsilon} \tag{14}$$

$$\frac{\partial \left(\bar{\rho}\,\tilde{\epsilon}\right)}{\partial t} + \nabla \cdot \left(\bar{\rho}\,\tilde{\vec{U}}\,\tilde{\epsilon}\right) = \nabla \cdot \left(\left[\mu + \frac{\mu_t}{\sigma_\epsilon}\right] \nabla \tilde{\epsilon}\right) + \frac{\tilde{\epsilon}}{\tilde{k}} \left(C_{\epsilon 1} P - C_{\epsilon 2}\, \bar{\rho} \tilde{\epsilon}\right) \tag{15}$$

where P (the production of $\tilde{k}$) is calculated from

$$P = 2\,\mu_t \left(\tilde{\vec{\vec{S}}} : \tilde{\vec{\vec{S}}} - \frac{1}{3}\left[\nabla \cdot \tilde{\vec{U}}\right]^2\right) - \frac{2}{3}\,\bar{\rho}\,k\,\left(\nabla \cdot \tilde{\vec{U}}\right) \tag{16a}$$

$$\tilde{\vec{\vec{S}}} \equiv \frac{1}{2}\left(\nabla \tilde{\vec{U}} + \nabla \tilde{\vec{U}}^{\,T}\right) \tag{16b}$$

The constants in Equations (13-15) are

$$C_\mu = 0.09,\ \sigma_k = 1,\ \sigma_\epsilon = 1.3,\ C_{\epsilon 1} = 1.6,\ C_{\epsilon 2} = 1.92$$

The standard value of $C_{\epsilon 1} = 1.44$ is modified to 1.6 in accordance with the McGuirk-Rodi [14] modification for self-similar round jets. The standard value tends to overestimate the spreading and decay rates for round jets. Dally et al. [15] showed that this modification outperforms the more complex modifications of Morse [16] or Pope [17] for an isothermal propane round jet. In addition, a constant value of $C_{\epsilon 1} = 1.6$ leads to better stability during the solver iterations [18]. The improved prediction of the spreading rate by modifying $C_{\epsilon 1}$ was also observed with a Reynolds stress model applied to a bluff-body methane/hydrogen flame simulation [19].

3 Computational Methods

The present computational study used a modified version of the *reactingFoam* application distributed as part of the finite volume library, OpenFOAM [20, 21] (Open Field Operation And Manipulation, version 1.5). The modified version of *reactingFoam* adds the term in the energy equation, Equation (4), due to the difference in the effective species and thermal diffusivities which was neglected in the version found in the OpenFOAM distribution.

The problem is solved assuming symmetry about the centerline. The computational domain extends for 400mm after the burner nozzle, and 196mm from the centerline. The structured mesh is nonuniform in the axial direction with a stretching factor of 1.01557. In the radial direction, the cells are uniform in the fuel-jet and the burner-tube thickness. The radial cell size (Δr) in these regions are 0.229mm and 0.22mm, respectively. In the air coflow, Δr is stretched away from the burner tube, with a minimum size of 0.22mm for the cell adjacent to the burner. The mesh has 13,050 cells and 26,576 points. There are 150 cells along the axial direction and 87 cells along the radial direction. The smallest axial mesh size (Δx) is at the burner-tube exit (0.6803mm). The mesh (in the $x - r$ domain) is illustrated in Figure 2, which shows a coarsened view of the mesh where only every third mesh line is shown in either direction. Therefore, each cell which is shown represents nine cells. Figure 3 shows a close-up of the mesh annotated with the burner tube and the air coflow. As shown in the figure, there are 10 cells along the inner radius of the fuel jet and 4 cells along the burner-tube thickness.

The PISO (Pressure Implicit Splitting of Operators) scheme was used to solve the governing equations of the reacting flow. The governing equations are corrected 5 times per time step. In each 'outer-loop' correction, there are 2 PISO corrections. Thus, the momentum, species-mass, and energy equations are solved 5 times per time step and pressure/momentum coupling and mass fluxes are corrected 10 times during a time step. The algebraic systems resulting from the discretized equations are solved iteratively through an 'inner loop' for each equation, with a tolerance of 10^{-12}. The bi-conjugate gradient (BiCG) iterative method is used with diagonal incomplete-LU preconditioning. A variable time step was adjusted dynamically to limit the maximum CFL (Courant-Friedrichs-Lewy) number to 0.5. The time step, (Δt), evolved to approximately 1.62×10^{-6} as the solution approached steady state. The backward Euler scheme was used for the time integration of the governing equations. Second order NVD (Normalized Variable Diagram) schemes (self-filtered central difference and gamma scheme) were used for the convective terms. Linear (second-order central difference) interpolation was used to calculate the mass fluxes at the face centers from the cell values, and was also used for calculating the diffusion terms.

The calculation of the non-normalized species reaction rate, RR_i requires the integration of a set of ordinary differential equations for the species, temperature and pressure within each cell in the domain. We used the fifth-order Runge-Kutta method of Cash and Karp [22] with fourth-order error control to solve the coupled system. With the specified error tolerances (5×10^{-6}) for the integration and specified limitation on the time step, this ODE solver was not able to perform the integration over the entire simulation time in the case of the 3-step (2009) kinetic model, so we used the semi-implicit Bulirsch-Stoer (SIBS) ODE solver [23]. It is based on Richardson extrapolation of the approximate solution. Neither of these ODE solvers would work successfully using the 3-step (2006) kinetic model, so the

implicit Euler scheme was selected.

The fuel-jet velocity profile at the exit of the burner tube is taken from the measurements. A uniform velocity (0.7m/s) is specified for the air coflow. Similarly, the inflow temperatures for the fuel-jet and air coflow are specified based on the experimental setting (i.e., 292 K for the jet and 290 K for the coflow). The exit pressure is specified (10^5 Pa), whereas a zero-gradient pressure condition is imposed at the inlet. The wall-function treatment is utilized at the walls. The fuel-jet and air coflow compositions are specified in terms of the species mass fractions. Based on the information provided by Sandia, we calculated these mass fractions and found them to be

$$Y_{CO,\text{jet}} = 0.55446, \quad Y_{H2,\text{jet}} = 0.02970, \quad Y_{N2,\text{jet}} = 0.41584 \tag{17}$$

in the jet, and

$$Y_{O2,\text{coflow}} = 0.22884, \quad Y_{N2,\text{coflow}} = 0.76363, \quad Y_{H2O,\text{coflow}} = 0.00753 \tag{18}$$

in the coflow.

4 Kinetic Models

We consider eight kinetic models (or reaction mechanisms), which are described here. The first three kinetic models consist of 2 or 3 global reactions. The reactions in these models have non-stoichiometric reaction orders with respect to the individual species. The remaining five kinetic models consist of 9, 21, 34, 37, or 38 elementary reactions. The reaction-rate constant (k) of each reaction step are prescribed in terms of the Arrhenius parameters: pre-exponential factor (A), temperature exponent (n), and activation energy (E), where

$$k = A\, T^n \exp\left(\frac{-E}{RT}\right) \tag{19}$$

The complete listing of the reaction steps and rates are tabulated in Appendices A-H. The units used for these data are mole, cm^3, second, K, and calorie (cal); which are the default units for the CHEMKIN-III software [24]. The rate-constant parameters that are originally published in other units are converted to these units. The universal gas constant (R) is 1985.89 cal/mol-K. With the exception of the 9-step kinetic model, the reverse-rate constants (for reversible reactions) are determined from the forward-rate and equilibrium constants. When the third-body (M) efficiencies are not given, they are equally unity. In the following subsections we provide a brief description of each kinetic model used in this study.

4.1 2-Step Kinetic Model: Slavinskaya et al. (2005)

This kinetic model consists of 2 global irreversible reactions with 5 species. It was proposed by Slavinskaya et al. [25, 26] who developed kinetic models for syngas combustion in stationary gas turbines. The kinetic model was validated on the base of laminar flame speed data. The 2 global steps and corresponding reaction rates are given in Appendix A.

4.2 3-Step Kinetic Model: Watanabe & Otaka (2006)

This kinetic model consists of 3 global reactions (one irreversible and two reversible) with 5 species. Watanabe and Otaka [27] proposed this kinetic model by combining the reversible H_2 oxidation and water-gas shift reactions of Jones and Lindstedt [28] (1988), with the irreversible CO oxidation of Westbrook and Dryer [29] (1981). In their work, Watanabe and Otaka [27] used this syngas kinetic model with two other global reactions for CH_4 to describe the reaction of the volatiles released from the pyrolysis of coal and gasification of char particles. The 3 global steps and corresponding reaction rates are given in Appendix B.

4.3 3-Step Kinetic Model: Cuoci et al. (2009)

This kinetic model consists of 3 global irreversible reactions with 5 species. Similar to the kinetic model of Watanabe and Otaka [27], Cuoci et al. [30] also started from the generic 3-step global kinetic model of Westbrook and Dryer [29] (1981) for hydrocarbons. However, instead of partially combining this model with the 4-step global kinetic model of Jones and Lindstedt [28] (1988), they replaced the hydrocarbon oxidation step with an H_2 oxidation step (the Westbrook-Dryer [29] kinetic model lacks such reaction) and optimized the rate-constant parameters. The optimization targets were laminar counter-flow flames at different strain rates (from $10s^{-1}$ to the extinction) and different fuel compositions. The 3 global steps and corresponding reaction rates are given in Appendix C.

4.4 9-Step Kinetic Model: Edelman & Fortune (1969)

This kinetic model consists of 9 elementary reversible reactions with 8 species. Edelman and Fortune [31] proposed a generic kinetic model for the combustion of paraffin fuels ($C_n\,H_{2n+2}$). Their kinetic model was proposed for turbulent burning in hypersonic engines and nozzles. In addition to the 9-step kinetic model we examine here, they proposed a global oxidation step for the paraffin fuel. The overall 10-step kinetic model was referred to by the authors as 'quasi-global mechanism'. We omit the global oxidation step and only apply the intermediate 9-step kinetic model. Edelman and Fortune [31] validated the quasi-global kinetic model against temperature histories from a detailed 69-step kinetic model and against shock tube ignition delay experiments for propane/oxygen and n-octane/oxygen systems (diluted by 80% to 99% argon) with different initial temperatures, pressures, and stoichiometric ratios. The authors commented that more comparisons are desirable, however they performed comparisons and established the creditability of their quasi-global kinetic model concept. The 9 elementary steps and corresponding parameters of the forward and reverse reaction-rate constants are given in Appendix D.

4.5 21-Step Kinetic Model: Westbrook & Dryer (1981)

This kinetic model consists of 21 elementary reversible reactions with 10 species. In the same study where Westbrook and Dryer [29] proposed their generic 3-step global kinetic model for hydrocarbons (using a numerical laminar flame model), they also presented an intermediate CO-H_2-O_2 kinetic model, which is the one described here. This intermediate kinetic model

was intended to be a generic model to be combined with a global oxidation reaction of n-paraffin fuels, which is similar to the approach used by Edelman and Fortune [31] mentioned earlier. Westbrook and Dryer [29] examined the performance of their quasi-global 22-step kinetic model by comparing the predicted species mole fractions and temperature profiles for a stoichiometric methanol-air mixture at atmospheric pressure with both the simplified and more detailed (84 elementary steps with 26 species) mechanism. Both kinetic models correctly reproduced the laminar flame speed. The temperature profile and concentration profiles of O_2, CO_2, and H_2O were in fairly good agreement. The 21 elementary steps and corresponding parameters of the forward reaction-rate constants are given in Appendix E.

4.6 34-Step Kinetic Model: Frassoldati et al. (2007)

This kinetic model consists of 34 (a duplicate reaction was counted as two reactions) elementary reactions (30 reversible and 4 irreversible) with 14 species. Frassoldati et al. [32] in 2006 presented a 21-step kinetic model for H_2 oxidation. With attention on operating conditions relevant to gas turbine applications, the same authors extended in 2007 [33] this kinetic model to H_2/CO by adding 3 species (CO, CO_2, and HCO) and 13 reactions. They validated their syngas kinetic model against a set of experimental measurements (including plug flow reactor, stirred reactor, shock tube and ignition delay times, laminar flame speeds, and ignition in a counter-flow flame) covering a wide range of operating conditions, principally under high-pressure conditions. In addition to converting the units, we updated and corrected (through personal communications with Professor Frassoldati) some rate-constant parameters that were published in the 2007 paper. The 34 elementary steps and corresponding parameters of the forward reaction-rate constants are given in Appendix F.

4.7 37-Step Kinetic Model: Politecnico di Milano (2008)

This kinetic model consists of 37 (a duplicate reaction was counted as two reactions) elementary reactions (30 reversible and 7 irreversible) with 14 species. It is in fact a slight extension of the 2007 Frassoldati et al. [33] kinetic model discussed in the previous subsection. In the present version of October-2008 (available online [34]), three H abstraction reactions were added. They are in the form

$$R + H_2 \rightarrow RH + H \tag{20a}$$

$$R + H_2O \rightarrow RH + OH \tag{20b}$$

$$R + H_2O_2 \rightarrow RH + HO_2 \tag{20c}$$

These added reactions and corresponding parameters of the forward reaction-rate constants are given in Appendix G.

4.8 38-Step Kinetic Model: University of Delaware (2003)

This kinetic model consists of 38 (four duplicate reactions were counted as eight reactions) reversible elementary reactions with 13 species. It is the last (and most detailed, in terms of the number of reaction steps) kinetic model we examine in this study. The kinetic model is

available online [35]. The 38 elementary steps and corresponding parameters of the forward reaction-rate constants are given in Appendix H.

5 Results

5.1 Computational Time

We begin by comparing the computational cost of the eight kinetic models in terms of the average CPU (execution) time per time step. We performed the timing on a single computing node, which has two processors, each of which is quad core Intel Xeon L5335 2.00GHz (total eight cores). The simulation using the 3-step (2009) model required 3.0389s per time step. This simulation required the shortest CPU time and was thus chosen to scale the CPU times for the remaining models. The 2-step model, requiring 3.1895s per time step, was the next lowest in terms of CPU time. However, it should be emphasized that chemistry was integrated using different ODE solvers. The absolute and relative elapsed CPU times are compared in Table 1. Comparing the computational times of the models which used the RK54 ODE solver, one can conclude, not surprisingly, that in general computational cost increases with the number of reaction-step (and species). The outlier is the 21-step model of Westbrook and Dryer [29], which, even on a coarser mesh, requires significantly more computational time than the simulation using the next slowest model.

Table 1: Average execution time per time step for different kinetic models (in ascending order of CPU time).

Kinetic model	# species	CPU time (sec)	CPU Ratio	ODE Solver
3-step (2009)	5	3.0389	1.00	SIBS
2-step	5	3.1895	1.05	RK54
9-step	8	6.8832	2.27	RK54
34-step	14	15.375	5.06	RK54
3-step (2006)	5	15.878	5.22	Euler Implicit
37-step	14	16.452	5.41	RK54
38-step	13	24.589	8.09	RK54
21-step*	10	114.81	37.8	RK54

* A different mesh (6,177 cells, 12,672 points) is utilized for this kinetic model because of its very long CPU time per time step.

5.2 Axial Profiles

The predicted Favre-averaged temperature fields from the simulations using eight kinetic models are shown in Figure 4. The flames predicted by the tested models differ in temper-

ature, size and shape (represented by the axial and radial extents of the high-temperature zone). The smallest flame is predicted by the 2-step model, whereas the largest flame is predicted by the 9-step model. The 2-step and 3-step (2009) models correspond to a reasonable flame length (the measured stoichiometric flame length was $\approx$ 215mm). The 9-step model predicts an extremely long flame. The other five models give a mildly long flame.

The axial profiles of the Favre-averaged temperature along the centerline using the eight kinetic models are compared in Figure 5. The simulations using the 3-step (2009) model provide the best agreement with the experimental temperature profile. The primary discrepancy is a slower predicted decay in the far downstream region. The measured peak temperature is 1919 K, which is only 9 K less than the predicted peak of 1928 K. The predicted peak temperature using the 2-step model is 1680 K, thus underpredicted by 239 K. However, its location (178mm after the burner) is in agreement with the measured one (183mm after the burner). The temperature profile using the 9-step model is considerably shallow, with a peak of 1342 K that is much less than the measured value. As the other five models give a similar temperature field to each other, they also overpredict the peak temperature and erroneously predict its location to be farther downstream than the measurements. The predicted peak temperature and its locations for the 3-step (2006), 21-step, 34-step, 37-step, and 38-step models are: 2240 K/282mm, 2162 K/282mm, 2163 K/282mm, 2115 K/272mm, and 2147 K/282mm, respectively. Adding the three abstraction reactions to the 34-step model improved the prediction of both the value and location of the peak temperature. Table 2 summarizes the predictions and deviations (predicted - measured) of the peak temperature and its location for the eight kinetic models.

Table 2: Predicted maximum centerline temperature and its location.

Kinetic model	Temperature (K)	Error (K)	Location (mm)	Error (mm)
2-step	1680	−239	178	−5
3-step (2006)	2240	+321	282	+99
3-step (2009)	1928	+9	211	+28
9-step	1342	−577	195	+12
21-step	2162	+243	282	+99
34-step	2163	+244	282	+99
37-step	2115	+196	272	+89
38-step	2147	+228	282	+99

The axial profiles of the Favre-averaged mass fraction of O_2 along the centerline using the eight kinetic models are compared in Figure 6. The increase in O_2 is due to mixing of co-flow into axis after the fuel is consumed. The extended region of low O_2 concentration for the 3-step (2006), 21-step, 34-step, 37-step, and 38-step models is due to the large flame sizes discussed earlier. Among the other models, the 3-step (2009) model has the least deviation from the measurements.

The axial profiles of the Favre-averaged mass fractions of CO and H_2 (the syngas species) along the centerline using the eight kinetic models are compared in Figures 7 and 8. All

models underpredict the axial decay of CO, but have better prediction of the axial decay of H_2.

The axial profiles of the Favre-averaged mass fraction of CO_2 and H_2O (the stable product species) along the centerline using the eight kinetic models are compared in Figures 9 and 10. Similar to the temperature profile, the mass fraction profiles predicted by the more detailed mechanisms are nearly identical. The particularly low CO_2 mass fractions calculated by the 2-step model would indicate that the temperature underprediction is due to incomplete oxidation of the CO. The incomplete oxidation of CO predicted by this model is due to the fact that formulated CO oxidation rate is dependent on the H_2 concentration.

6 Concluding Remarks

We numerically simulated the Sandia-ETH turbulent nonpremixed syngas flame (diluted by 30% nitrogen) using the finite volume method and the partially stirred reactor (PaSR) approach. The finite-rate chemistry in the perfectly stirred portion of the computational cells are described by eight different kinetic models (or reaction mechanisms), which consist of 2 global steps, 3 global steps (two models), 9 elementary steps, 21 elementary steps, 34 elementary steps, 37 elementary steps, and 38 elementary steps. We compared the prediction capability (in terms of axial Favre-averaged profiles) and computational demands (in terms of the simulation CPU time per time step) of these kinetic models.

The computational cost using the different kinetic models varies largely, with the 38-step and 21-step model having CPU times that are approximately 8 and 36 times those recorded for the 2-step and 3-step/2009 models. Models with a larger number of steps are not necessarily more computationally demanding. The actual rate formulas have important effect due to their direct influence on the concentration-rate ODE system. All models predict slower combustion of CO than the measurements. The 9-step model of Edelman and Fortune (1969) significantly underpredicts the flame temperature and overpredicts the flame length and width, which is not surprising since the model was developed for a different flame regime. It is completely not suitable for the simple turbulent flame examined here. The 2-step model of Slavinskaya et al. (2005) is also not suitable for the present syngas flame because the rate of CO oxidation is dependent of H_2. The 3-step model of Watanabe & Otaka (2006), 21-step model of Westbrook & Dryer (1981), 34-step model of Frassoldati et al. (2007), 37-step model of Politecnico di Milano (2008), and 38-step model of the University of Delaware (2003) share several characteristics, such as overpredicting the peak temperature and its downstream location. The 3-step kinetic model of Cuoci et al. (2009) provided the more accurate prediction of the flame. It was also the model with the lowest computational cost.

7 Acknowledgments

This research was supported in part by an appointment to the National Energy Technology Laboratory Research Participation Program, sponsored by the U.S. Department of Energy and administered by the Oak Ridge Institute for Science and Education.

Appendix A: 2-Step Kinetics, Slavinskaya et al. (2005)

Table 3: Reactions and rate data. Units are: mol, cm^3, sec, K, cal.

Step	Reaction	Rate
1	$2H_2 + O_2 \rightarrow 2H_2O$	10.8e-7 $T^{6.1}$ $\exp(-9,684.5/\Re T)[H_2]^2$
2	$CO + H_2 + O_2 \rightarrow CO_2 + H_2O$	20.15e-8 $T^{5.9}$ $\exp(-6,097.6/\Re T)[O_2][CO]^{1.4}$

Appendix B: 3-Step Kinetics, Watanabe & Otaka (2006)

Table 4: Reactions and rate data. Units are: mol, cm^3, sec, K, cal.

Step	Reaction	Rate (forward)
1	$H_2 + 0.5O_2 \rightleftharpoons H_2O$	1.209e18 T^{-1} $\exp(-40,000/\Re T)[H_2]^{0.25}[O_2]^{1.5}$
2	$CO + 0.5O_2 \rightarrow CO_2$	3.981e14 $\exp(-40,000/\Re T)[CO][O_2]^{0.25}[H_2O]^{0.5}$
3	$CO + H_2O \rightleftharpoons CO_2 + H_2$	2.75e12 $\exp(-20,000/\Re T)[CO][H_2O]$

Appendix C: 3-Step Kinetics, Cuoci et al. (2009)

Table 5: Reactions and rate data. Units are: mol, cm^3, sec, K, cal.

Step	Reaction	Rate
1	$CO + 0.5O_2 \rightarrow CO_2$	2.3e14 $\exp(-31,700/\Re T)[CO][H_2O]$
2	$CO_2 \rightarrow CO + 0.5O_2$	4.45e9 $\exp(-41,300/\Re T)[CO_2]$
3	$H_2 + 0.5O_2 \rightarrow H_2O$	1.097e11 $\exp(-6,900/\Re T)[H_2]^{0.87}[O_2]^{1.1}$

Appendix D: 9-Step Kinetics, Edelman & Fortune (1969)

Table 6: Reactions and rate data. Units are: mol, cm^3, sec, K, cal.

Step	Reaction	A	n	E
1	$CO + OH \rightleftharpoons CO_2 + H$	3.2e12	0	3,170.6
	(Reverse)	2.7e17	-0.79	15,450
2	$OH + H_2 \rightleftharpoons H + H_2O$	6.3e13	0	2,969.3
	(Reverse)	2.4e14	0	10,413
3	$OH + OH \rightleftharpoons H_2O + O$	7.6e12	0	503.27
	(Reverse)	6.9e13	0	8,928
4	$O + H_2 \rightleftharpoons OH + H$	3.3e12	0	3,593.4
	(Reverse)	1.4e12	0	2,612
5	$H + O_2 \rightleftharpoons OH + O$	2.4e14	0	8,429.8
	(Reverse)	3.2e11	0.47	50.32
6	$O + H + M \rightleftharpoons OH + M$	3.0e14	0	0
	(Reverse)	7.5e14	0.06	50,976
7	$O + O + M \rightleftharpoons O_2 + M$	2.2e13	0	0
	(Reverse)	2.5e16	-0.5	59,336
8	$H + H + M \rightleftharpoons H_2 + M$	2.0e18	-1	0
	(Reverse)	2.4e19	-0.86	51,958
9	$H + OH + M \rightleftharpoons H_2O + M$	2.3e21	-1.5	0
	(Reverse)	1.2e23	-1.34	59,399.6

Appendix E: 21-Step Kinetics, Westbrook & Dryer (1981)

Table 7: Reactions and rate data. Units are: mol, cm^3, sec, K, cal.

Step	Reaction	A	n	E
1	$H + O_2 \rightleftharpoons O + OH$	2.2e14	0	16,800
2	$H_2 + O \rightleftharpoons H + OH$	1.8e10	1	8,900
3	$O + H_2O \rightleftharpoons OH + OH$	6.8e13	0	18,400
4	$OH + H_2 \rightleftharpoons H + H_2O$	2.2e13	0	5,100
5	$H + O_2 + M \rightleftharpoons HO_2 + M$	1.5e15	0	-1,000
6	$O + HO_2 \rightleftharpoons O_2 + OH$	5e13	0	1,000
7	$H + HO_2 \rightleftharpoons OH + OH$	2.5e14	0	1,900
8	$H + HO_2 \rightleftharpoons H_2 + O_2$	2.5e13	0	700
9	$OH + HO_2 \rightleftharpoons H_2O + O_2$	5e13	0	1,000
10	$HO_2 + HO_2 \rightleftharpoons H_2O_2 + O_2$	1e13	0	1,000
11	$H_2O_2 + M \rightleftharpoons OH + OH + M$	1.2e17	0	45,500
12	$HO_2 + H_2 \rightleftharpoons H_2O_2 + H$	7.3e11	0	18,700
13	$H_2O_2 + OH \rightleftharpoons H_2O + HO_2$	1e13	0	1,800
14	$CO + OH \rightleftharpoons CO_2 + H$	1.5e7	1.3	-800
15	$CO + O_2 \rightleftharpoons CO_2 + O$	3.1e11	0	37,600
16	$CO + O + M \rightleftharpoons CO_2 + M$	5.9e15	0	4,100
17	$CO + HO_2 \rightleftharpoons CO_2 + OH$	1.5e14	0	23,700
18	$OH + M \rightleftharpoons O + H + M$	8e19	-1	103,700
19	$O_2 + M \rightleftharpoons O + O + M$	5.1e15	0	115,000
20	$H_2 + M \rightleftharpoons H + H + M$	2.2e14	0	96,000
21	$H_2O + M \rightleftharpoons H + OH + M$	2.2e16	0	105,000

Appendix F: 34-Step Kinetics, Frassoldati et al. (2007)

Table 8: Reactions and rate data. Units are: mol, cm^3, sec, K, cal.

Step	Reaction	A	n	E
1	$H + O_2 \rightleftharpoons OH + O$	2.21e14	0	16,650
2	$O + H_2 \rightleftharpoons OH + H$	4.33e13	0	10,000
3	$H + O_2\ (+M) \rightleftharpoons HO_2\ (+M)$	4.65e12	0.4	0
	Low	7e17	-0.8	0
	Troe : 0.5; $1e$-30; $1e30$			
	$M : H_2O = 18, H_2 = 2.5, N_2 = 1.26,$			
	$O_2 = 0, Ar = 0.8, He = 0.8,$			
	$CO = 1.2, CO_2 = 2.4$			
4	$H + O_2 + O_2 \rightleftharpoons HO_2 + O_2$	8.9e14	0	-2,822
5	$OH + HO_2 \rightleftharpoons H_2O + O_2$	5e13	0	1,000
6	$H + HO_2 \rightleftharpoons OH + OH$	2.5e14	0	1,900
7	$O + HO_2 \rightleftharpoons O_2 + OH$	3.25e13	0	0
8	$OH + OH \rightleftharpoons O + H_2O$	3.57e4	2.4	-2,110
9	$H_2 + M \rightleftharpoons H + H + M$	2.23e14	0	96,081
	$M : H_2O = 12, H_2 = 2.5, CO = 1.9,$			
	$CO_2 = 3.8, Ar = 0.5, He = 0.5$			
10	$O_2 + M \rightleftharpoons O + O + M$	1.55e14	0	115,120
	$M : H_2O = 12, H_2 = 2.5, CO = 1.9,$			
	$CO_2 = 3.8, Ar = 0.2, He = 0.2$			
11	$H + OH + M \rightleftharpoons H_2O + M$	4.5e22	-2	0
	$M : H_2O = 16, H_2 = 2, CO = 1.9$			
12	$H + HO_2 \rightleftharpoons H_2 + O_2$	2.5e13	0	700
13	$HO_2 + HO_2 \rightleftharpoons H_2O_2 + O_2$	2.11e12	0	0
14	$OH + OH\ (+M) \rightleftharpoons H_2O_2\ (+M)$	7.4e13	-0.37	0
	Low	2.3e18	-0.9	-1,700
	Troe : 0.7346; 94; $1,756$; $5,182$			
	$M : H_2O = 6, H_2 = 2, CO = 1.5,$			
	$CO_2 = 2, Ar = 0.7, He = 0.7$			
15	$O + OH + M \rightleftharpoons HO_2 + M$	1e16	0	0
16	$H + H_2O \rightleftharpoons H_2 + OH$	4e10	1	19,000
17	$H_2O_2 + H \rightleftharpoons H_2O + OH$	2.41e13	0	3,970
18	$H_2O_2 + H \rightleftharpoons H_2 + HO_2$	6.025e13	0	7,950

Reactions and rate data (continued).

Step	Reaction	A	n	E
19	$HO_2 + H_2O \rightarrow H_2O_2 + OH$	5.388e5	2	28,780
20	$OH + H_2O_2 \rightarrow H_2O + HO_2$	3.195e5	2	-4,169.95
21	$O + H_2O_2 \rightarrow OH + HO_2$	1.083e6	2	-1,657.32
22	$CO + O\ (+M) \rightleftharpoons CO_2\ (+M)$	9.64e10	0	3,800
	Low	2.07e26	-3.34	7,610
	$M : H_2O = 12, H_2 = 2, CO = 1.5,$ $CO_2 = 2, Ar = 0.5$			
23	$CO + OH \rightleftharpoons CO_2 + H$	9.6e11	0.14	7,352
24	Duplicate of (23)	7.32e10	0.03	-16
25	$CO + HO_2 \rightleftharpoons CO_2 + OH$	3e13	0	23,000
26	$CO + H_2O \rightleftharpoons CO_2 + H_2$	2e11	0	38,000
27	$O_2 + CO \rightleftharpoons CO_2 + O$	2.53e12	0	47,700
28	$HCO + M \rightleftharpoons CO + H + M$	1.2e17	-1	17,000
	$M : H_2O = 5, H_2 = 1.9, CO = 1.9,$ $CO_2 = 3$			
29	$HCO + O \rightleftharpoons CO_2 + H$	3e13	0	0
30	$HCO + H \rightleftharpoons H_2 + CO$	1e14	0	0
31	$HCO + OH \rightleftharpoons H_2O + CO$	5e13	0	0
32	$HCO + HO_2 \rightleftharpoons H_2O_2 + CO$	4e11	0	0
33	$O_2 + HCO \rightleftharpoons HO_2 + CO$	1e12	0	0
34	$HCO + HO_2 \rightarrow H + OH + CO_2$	3e13	0	0

Appendix G: 37-Step Kinetics, Politec. di Milano (2008)

The following reaction information needs to be augmented with the one in Appendix F (34 reactions).

Table 9: Reactions and rate data (in addition to those in Table 8). Units are: mol, cm^3, sec, K, cal.

Step	Reaction	A	n	E
35	$H + H_2 \rightarrow H_2 + H$	3.003e7	2	7,658.6
36	$OH + H_2O \rightarrow H_2O + OH$	3.994e6	2	2,223.39
37	$HO_2 + H_2O_2 \rightarrow H_2O_2 + HO_2$	4.31e4	2	5,529.49

Appendix H: 38-Step Kinetics, Univ. of Delaware (2003)

Table 10: Reactions and rate data. Units are: mol, cm^3, sec, K, cal.

Step	Reaction	A	n	E
1	$H + O_2 \rightleftharpoons O + OH$	2.644e16	-0.6707	17,041
2	$O + H_2 \rightleftharpoons H + OH$	4.589e4	2.7	6,260
3	$OH + H_2 \rightleftharpoons H + H_2O$	1.734e8	1.51	3,430
4	$OH + OH \rightleftharpoons O + H_2O$	3.973e4	2.4	-2,110
5	$H + H + M \rightleftharpoons H_2 + M$	1.78e18	-1	0
	$M : Ar = 0.63, He = 0.63$			
6	$H + H + H_2 \rightleftharpoons H_2 + H_2$	9e16	-0.6	0
7	$H + H + H_2O \rightleftharpoons H_2 + H_2O$	5.624e19	-1.25	0
8	$H + H + CO_2 \rightleftharpoons H_2 + CO_2$	5.5e20	-2	0
9	$H + OH + M \rightleftharpoons H_2O + M$	4.4e22	-2	0
	$M : H_2 = 2, H_2O = 6.3, CO = 1.75,$			
	$CO_2 = 3.6, Ar = 0.38, He = 0.38$			
10	$O + H + M \rightleftharpoons OH + M$	9.428e18	-1	0
	$M : H_2 = 2, H_2O = 12, CO = 1.75,$			
	$CO_2 = 3.6, Ar = 0.7, He = 0.7$			
11	$O + O + M \rightleftharpoons O_2 + M$	1.2e17	-1	0
	$M : H_2 = 2.4, H_2O = 15.4, CO = 1.75,$			
	$CO_2 = 3.6, Ar = 0.83, He = 0.83$			
12	$H + O_2\ (+M) \rightleftharpoons HO_2\ (+M)$	5.116e12	0.44	0
	Low	6.328e19	-1.4	0
	Troe : 0.5; 1e-30; 1e30			
	$M : O_2 = 0.85, H_2 = 0.75, H_2O = 11.89,$			
	$CO = 1.09, CO_2 = 2.18,$			
	$Ar = 0.4, He = 0.46$			
13	$H_2 + O_2 \rightleftharpoons HO_2 + H$	5.916e5	2.433	53,502
14	$OH + OH\ (+M) \rightleftharpoons H_2O_2\ (+M)$	1.11e14	-0.37	0
	Low	2.01e17	-0.584	-2,293
	Troe : 0.7346; 94; 1,756; 5,182			
	$M : H_2 = 2, H_2O = 6, CO = 1.75,$			
	$CO_2 = 3.6, Ar = 0.7, He = 0.7$			
15	$HO_2 + H \rightleftharpoons O + H_2O$	3.97e12	0	671

Reactions and rate data (continued).

Step	Reaction	A	n	E
16	$HO_2 + H \rightleftharpoons OH + OH$	7.485e13	0	295
17	$HO_2 + O \rightleftharpoons OH + O_2$	4e13	0	0
18	$HO_2 + OH \rightleftharpoons O_2 + H_2O$	2.375e13	0	-500
19	Duplicate of (18)	1e16	0	17,330
20	$HO_2 + HO_2 \rightleftharpoons O_2 + H_2O_2$	1.3e11	0	-1,630
21	Duplicate of (20)	3.658e14	0	12,000
22	$H_2O_2 + H \rightleftharpoons HO_2 + H_2$	6.05e6	2	5,200
23	$H_2O_2 + H \rightleftharpoons OH + H_2O$	2.41e13	0	3,970
24	$H_2O_2 + O \rightleftharpoons OH + HO_2$	9.63e6	2	3,970
25	$H_2O_2 + OH \rightleftharpoons HO_2 + H_2O$	2e12	0	427
26	Duplicate of (25)	2.67e41	-7	37,600
27	$CO + O\ (+M) \rightleftharpoons CO_2\ (+M)$	1.362e10	0	2,384
	Low	1.173e24	-2.79	4,191
	$M : H_2 = 2, H_2O = 12, CO = 1.75,$			
	$CO_2 = 3.6, Ar = 0.7, He = 0.7$			
28	$CO + OH \rightleftharpoons CO_2 + H$	8e11	0.14	7,352
29	Duplicate of (28)	8.784e10	0.03	-16
30	$CO + O_2 \rightleftharpoons CO_2 + O$	1.119e12	0	47,700
31	$CO + HO_2 \rightleftharpoons CO_2 + OH$	3.01e13	0	23,000
32	$HCO + H \rightleftharpoons CO + H_2$	1.2e14	0	0
33	$HCO + O \rightleftharpoons CO + OH$	3e13	0	0
34	$HCO + O \rightleftharpoons CO_2 + H$	3e13	0	0
35	$HCO + OH \rightleftharpoons CO + H_2O$	3.02e13	0	0
36	$HCO + M \rightleftharpoons CO + H + M$	1.87e17	-1	17,000
	$M : H_2 = 2, CO = 1.75, CO_2 = 3.6$			
37	$HCO + H_2O \rightleftharpoons CO + H + H_2O$	2.244e18	-1	17,000
38	$HCO + O_2 \rightleftharpoons CO + HO_2$	1.204e10	0.807	-727

References

[1] M. R. Beychok, *Environmental Protection Technology Series*, U.S. EPA Report, EPA-68-03-2136, 1975.

[2] R. S. Barlow, G. J. Fiechtner, C. D. Carter, M. Flury, *Sandia/ETH-Zurich $CO/H_2/N_2$ Flame Data - Release 1.1*, www.ca.sandia.gov/TNF, Sandia National Laboratories, 2002.

[3] R. S. Barlow, G. J. Fiechtner, C. D. Carter, J.-Y. Chen, *Combustion and Flame* 120 (2000) 549–569.

[4] M. Flury, *Experimentelle Analyse der Mischungstruktur in Turbulenten nicht Vorgemischten Flammen*, Ph.D. Dissertation, ETH Zurich, Switzerland, 1998.

[5] J. Panda, R. G. Seasholtz, *Proceedings of the AIAA Aerospace Sciences Meeting and Exhibit* (2005) AIAA-2005-514.

[6] T. Poinsot, D. Veynante, *Theoretical and Numerical Combustion*, 2nd Edition, R.T. Edwards, Inc., Philadelphia, PA, 2005.

[7] F. A. Maury, P. A. Libby, *Combustion and Flame* 102 (1995) 341–356.

[8] Z. Zhu, N. Stokes, *Proceedings of the International Conference on CFD in Mineral & Metal Processing and Power Generation* (1997) pp. 387–394.

[9] L. Vervisch, D. Veynante, *Progress in Energy and Combustion Science* 28 (2002) 193–266.

[10] L. A. Vulis, *Thermal Regimes of Combustion*, McGraw-Hill Book Company, Inc., New York, 1961.

[11] J. Chomiak, J. A. J. Karlsson, *Proceedings of the Twenty-Sixth Symposium (International) on Combustion* (1996) pp. 2557–2564.

[12] B. F. Magnussen, B. H. Hjertager, J. G. Oslen, D. Bhaduri, *Proceedings of the Seventeenth Symposium (International) on Combustion* (1978) pp. 1383–1393.

[13] I. R. Gran, B. F. Magnussen, *Combustion Science and Technology* 119 (1996) 191–217.

[14] J. J. McGuirk, W. Rodi, in: F. Durst, B. E. Launder, F. W. Schmidt, J. H. Whitelaw (Eds.), *Turbulent Shear Flows 1: Selected Papers from the First International Symposium on Turbulent Shear Flows*, 1979, pp. 71–83.

[15] B. B. Dally, D. F. Fletcher, A. R. Masri, *Combustion Theory and Modelling* 2 (1998) 193–219.

[16] A. P. Morse, *Axisymmetric Turbulent Shear Flows with and without Swirl*, Ph.D. Dissertation, London University, 1977.

[17] S. B. Pope, *AIAA Journal* 16 (1978) 279–281.

[18] M. Hossain, J. C. Jones, W. Malalasekera, *Flow, Turbulence and Combustion* 67 (2001) 217-234.

[19] A. Odedra, W. Malalasekera, *Combustion and Flame* 151 (2007) 512–531.

[20] OpenFOAM: The Open Source CFD Toolbox. Available from: http://www.openfoam.org

[21] H. G. Weller, G. Tabor, H. Jasak, C. Fureby, Computers in Physics, 12 (1998) 620–631.

[22] J. R. Cash, A. H. Karp, *ACM Transactions on Mathematical Software* 16 (1990) 201–222.

[23] F. S. Acton, *Numerical Methods That Work*, 4th Printing, The Mathematical Association of America, Washington, D.C., 1990

[24] R. J. Kee, F. M. Rupley, E. Meeks, J. A. Miller, *CHEMKIN-III: A FORTRAN Chemical Kinetics Package for the Analysis of Gas-phase Chemical and Plasma Kinetics*, Sandia Report, SAND96-8216 • UC-405, 1996.

[25] N. Slavinskaya, M. Braun-Unkhoff, P. Frank, *Proceedings of the ASME Turbo Expo* (2005) GT2005–68287.

[26] N. Slavinskaya, M. Braun-Unkhoff, P. Frank, *Journal of Engineering for Gas Turbines and Power* 130 (2008) 021504,1–6.

[27] H. Watanabe, M. Otaka, *Fuel* 85 (2006) 1935–1943.

[28] W. P. Jones, R. P. Lindstedt, *Combustion and Flame* 73 (1988) 233–249.

[29] C. K. Westbrook, F. L. Dryer, *Combustion Science and Technology* 27 (1981) 31–43.

[30] A. Cuoci, A. Frassoldati, T. Faravelli, E. Ranzi, *Proceedings of the 32nd Combustion Meeting of the Italian Section of the Combustion Institute* (2009) II-6,1–6.

[31] R. B. Edelman, O. F. Fortune, *Proceedings of the AIAA 7th Aerospace Sciences Meeting* (1969) AIAA-1969-86.

[32] A. Frassoldati, T. Faravelli, E. Ranzi, *International Journal of Hydrogen Energy* 31 (2006) 2310–2328.

[33] A. Frassoldati, T. Faravelli, E. Ranzi, *International Journal of Hydrogen Energy* 32 (2007) 3471–3485.

[34] Chemical Reaction Engineering and Chemical Kinetics at Politecnico di Milano, Piazza, Italy. http://www.chem.polimi.it/CRECKModeling/kinetic.html

[35] Combustion Kinetics Laboratory - Aerospace and Mechanical Engineering, University of Southern California, Los Angeles. http://ignis.usc.edu/Mechanisms/H2-CO/h2-co.html

Figure 1: Photograph of the Sandia-ETH chnA flame.
(source: http://www.ca.sandia.gov/TNF/DataArch/SANDchn.html)

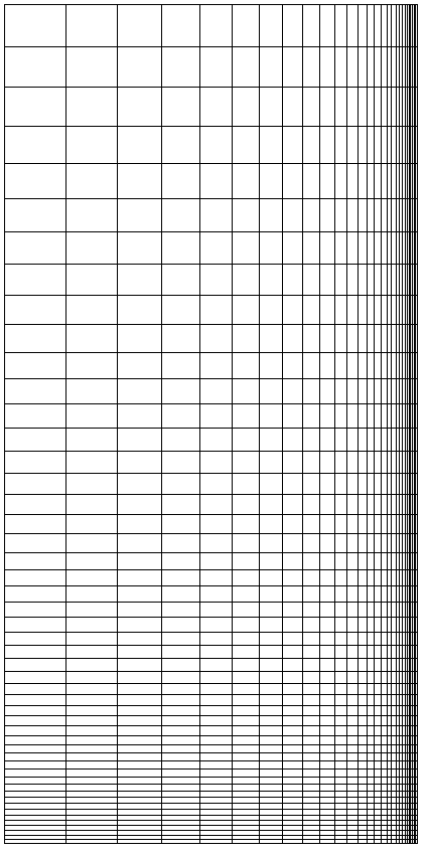

Figure 2: Illustration of the mesh (1/9 the number of cells is shown).

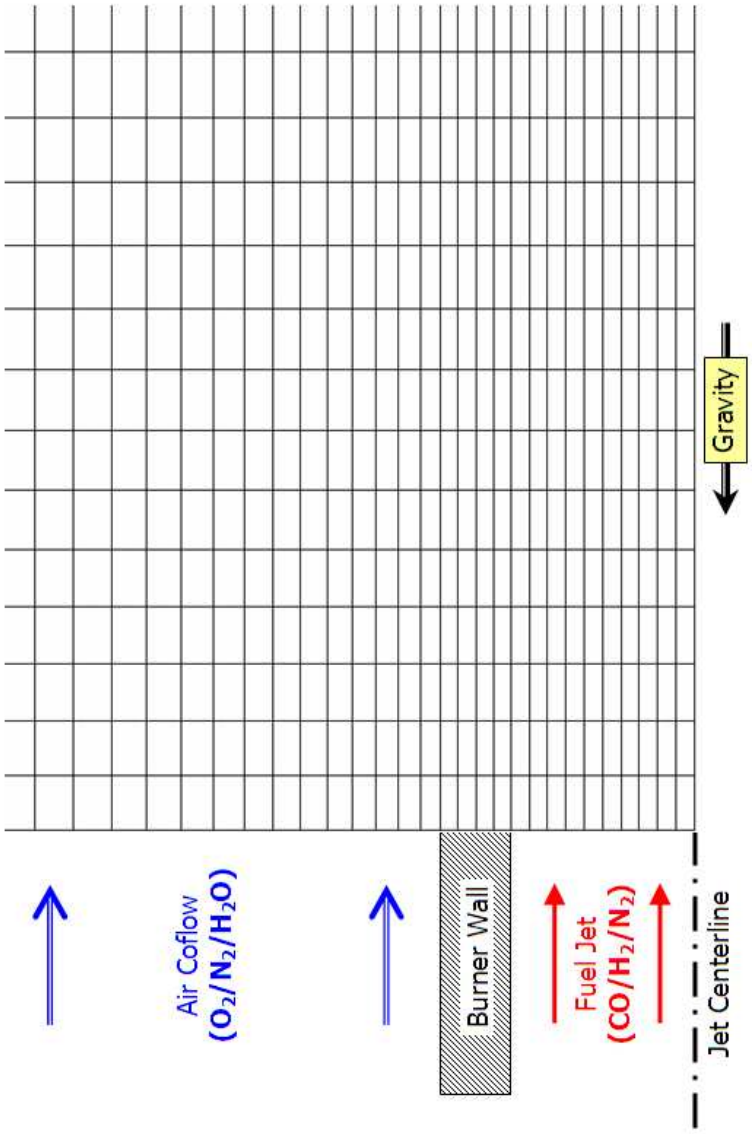

Figure 3: Illustration of the mesh near the inlet.

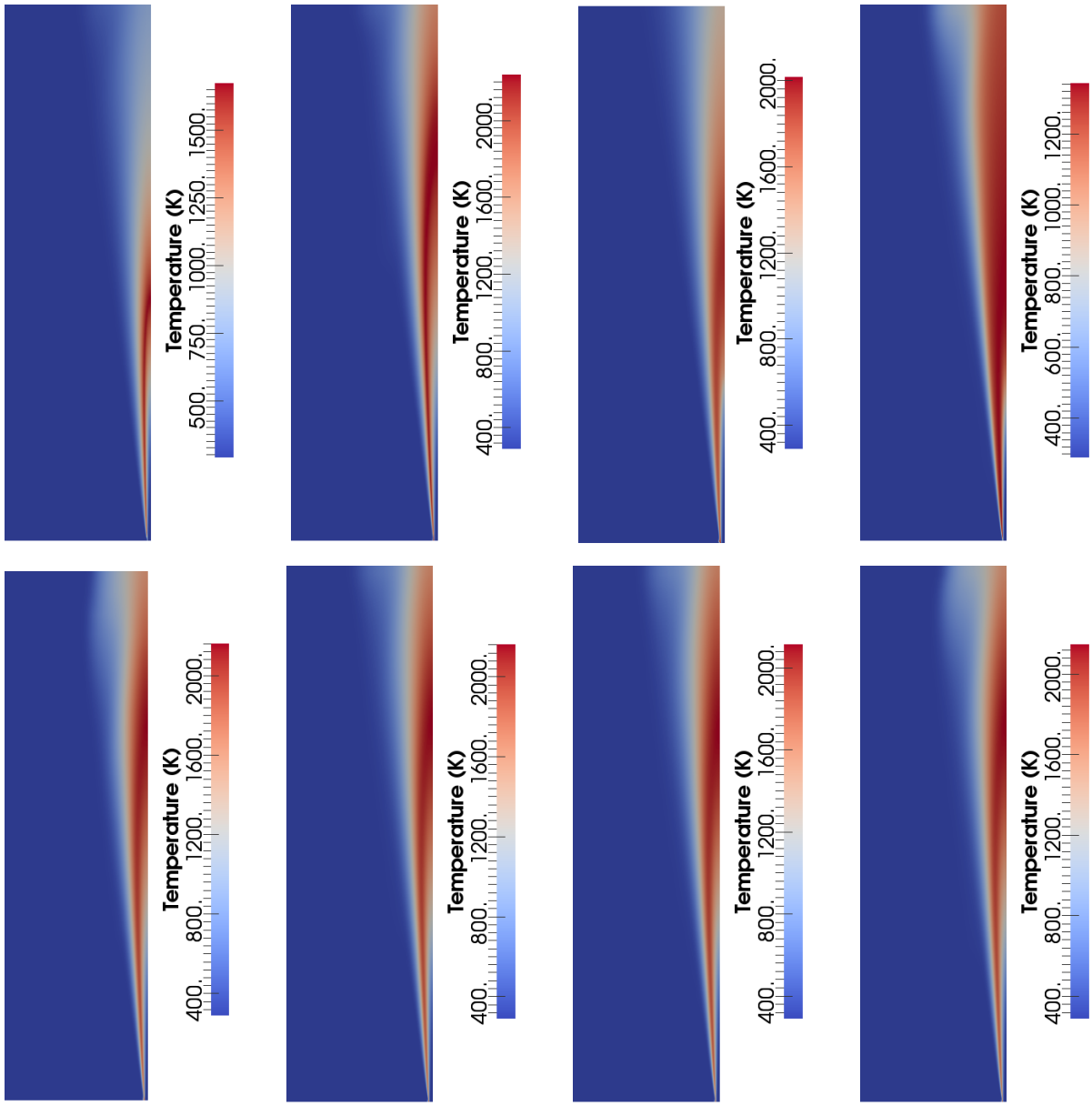

Figure 4: Mean temperature field, using different kinetic models.
Top (from left to right): 2-step, 3-step (2006), 3-step (2009), 9-step.
Bottom (from left to right): 21-step, 34-step, 37-step, 38-step.
The domain height is 400mm in each plot.

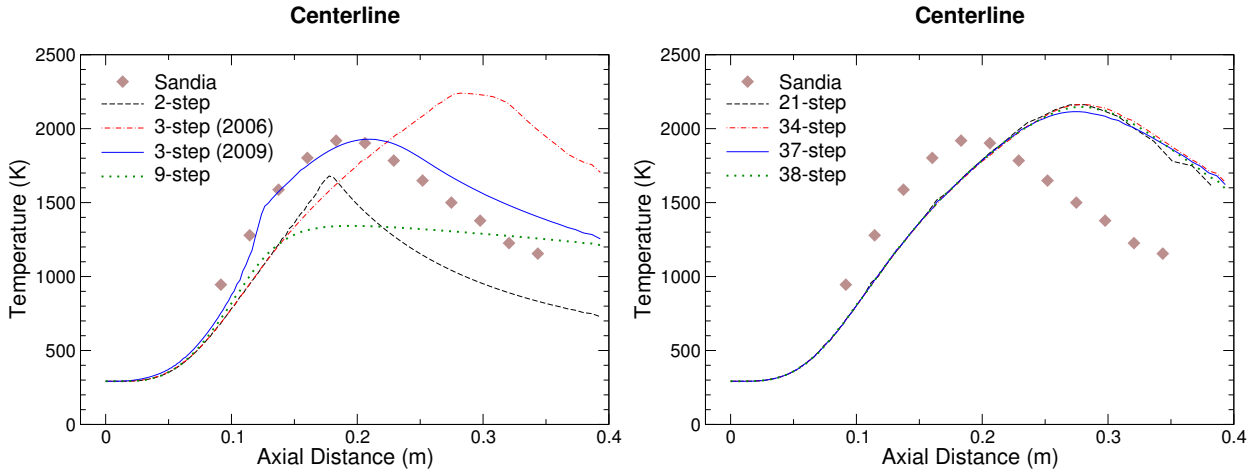

Figure 5: Mean temperature at centerline, using different kinetic models.

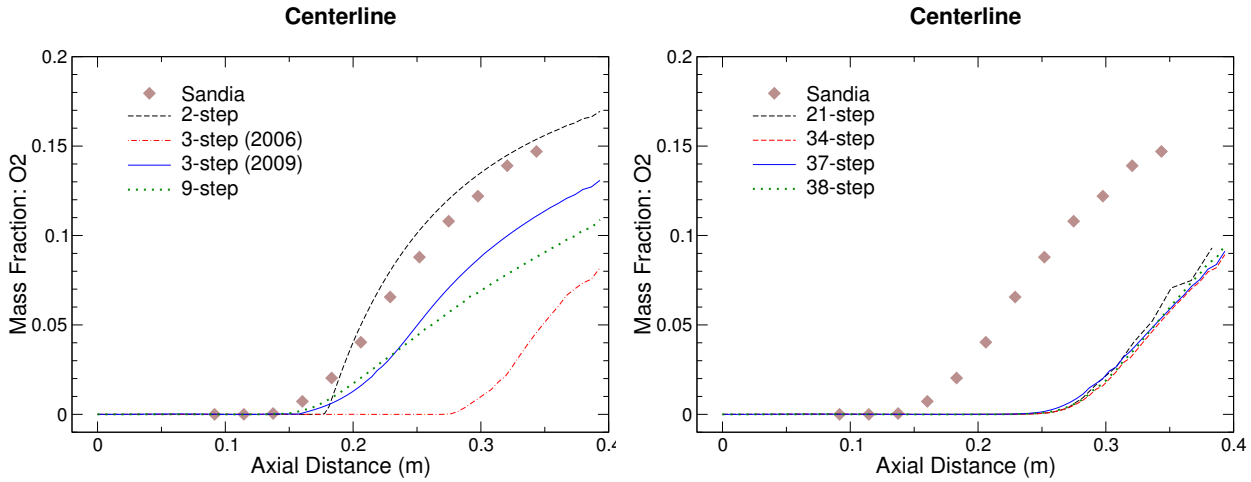

Figure 6: Mean O_2 mass fraction at centerline, using different kinetic models.

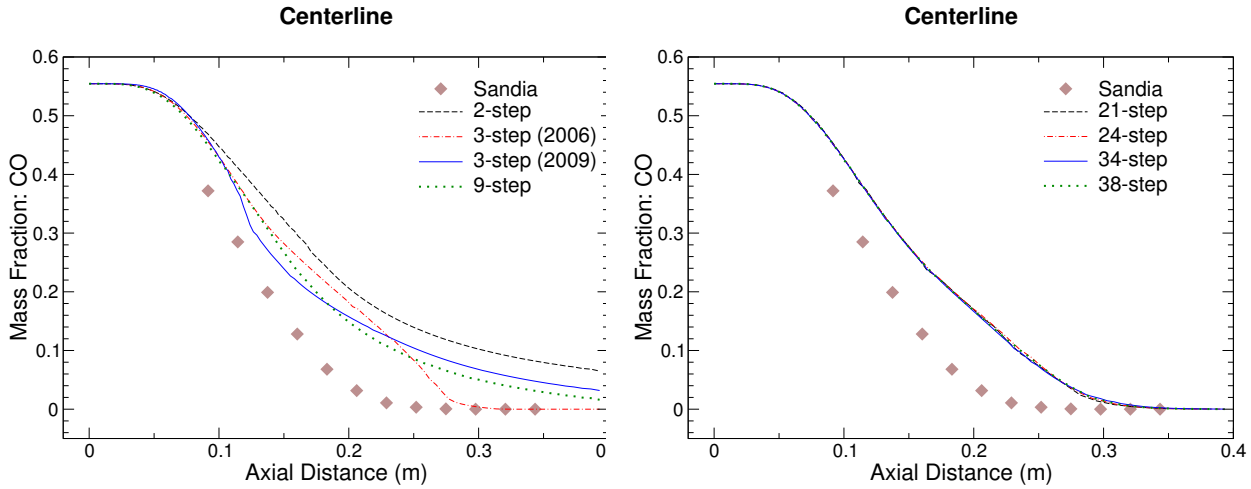

Figure 7: Mean CO mass fraction at centerline, using different kinetic models.

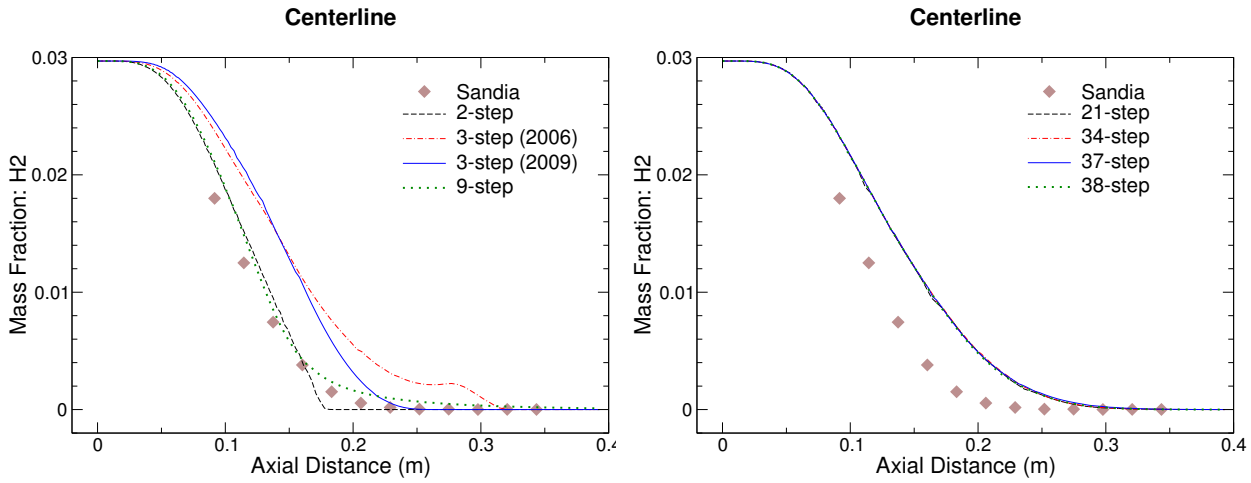

Figure 8: Mean H_2 mass fraction at centerline using, different kinetic models.

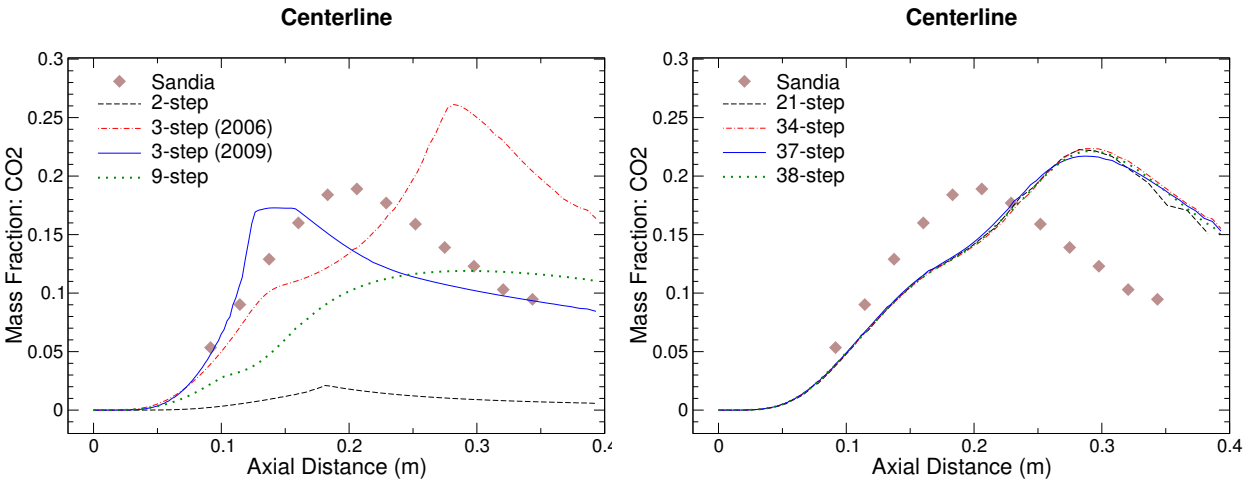

Figure 9: Mean CO_2 mass fraction at centerline, using different kinetic models.

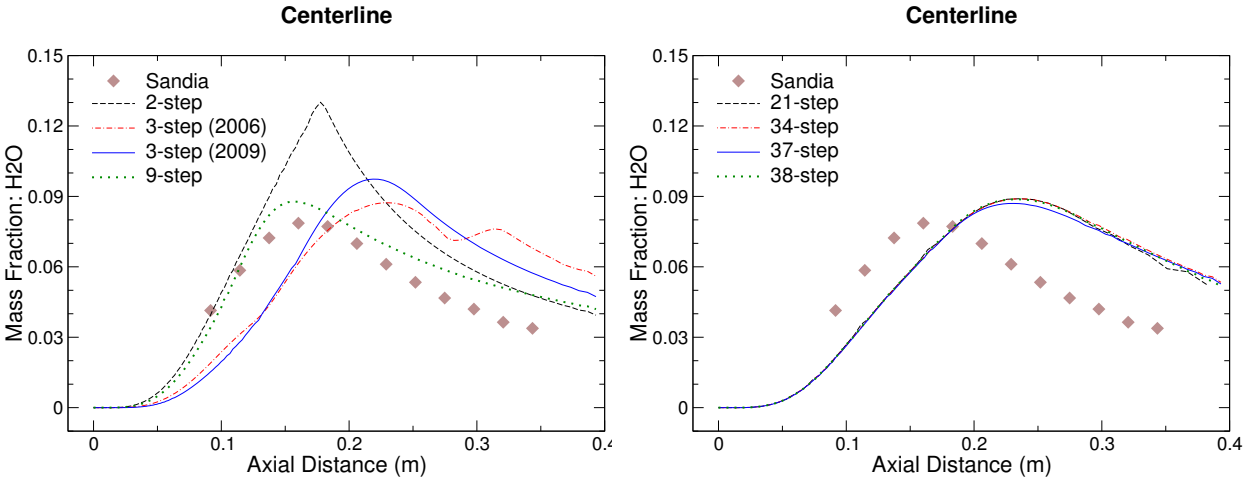

Figure 10: Mean H_2O mass fraction at centerline, using different kinetic models.